EVALUATION OF WARM-RAIN MICROPHYSICAL PARAMETERIZATIONS IN MESOSCALE SIMULATIONS OF THE CLOUDY MARINE BOUNDARY LAYER

BY

Kevin J. Nelson

Submitted to the graduate degree program in Geography and the Graduate Faculty of the University of Kansas in partial fulfillment of the requirements for the degree of Master of Science

---

David B. Mechem
Chairperson

David A. Rahn

Donna F. Tucker

Date Defended: June 26, 2015

The Thesis Committee for Kevin J. Nelson
certifies that this is the approved version of the following thesis:

EVALUATION OF WARM-RAIN MICROPHYSICAL PARAMETERIZATIONS IN MESOSCALE SIMULATIONS OF THE CLOUDY MARINE BOUNDARY LAYER

David B. Mechem
Chairperson

Date Approved: June 26, 2015

ABSTRACT

EVALUATION OF WARM-RAIN MICROPHYSICAL PARAMETERIZATIONS IN MESOSCALE SIMULATIONS OF THE CLOUDY MARINE BOUNDARY LAYER

Kevin J. Nelson

Department of Geography
Program in Atmospheric Science

Master of Science

Marine boundary layer clouds cool the climate system by influencing the shortwave radiation budget, and on shorter timescales can influence marine and aircraft operations. We evaluate the ability of a regional forecast model (NRL COAMPS) to accurately represent marine boundary layer cloud properties, using a number of different microphysical parameterizations. We focus on both the relative performance of the different parameterizations and on how they compare to observations from the VOCALS-REx field campaign conducted over the southeastern Pacific in 2008. We found evidence of a negative model bias on liquid water path (LWP) and marine boundary layer (MBL) depth, and persistent over-estimation of precipitation rates in mesoscale simulations. Certain aspects of the diurnal cycle of cloud systems were also observed. In addition to direct comparisons with the observations to evaluate forecast accuracy, we

assess the internal consistency of model microphysical properties by comparing simulation output to a number of observationally derived scalings for precipitation and aerosol scavenging. Model output holds well to the observationally derived scalings, and resolution plays a significant role in determining whether or not the model microphyics is consistent with observations.

ACKNOWLEDGMENTS

First, I would like to thank my advisor, Dr. David Mechem, for all of his support and patience throughout my time at the University of Kansas. I would also like to thank Dr. David Rahn and Dr. Donna Tucker for taking the time to serve on my thesis committee and for valuable insights into my research. Thank you to my collaborator, Dr. Yefim Kogan, for helpful comments on my thesis manuscript and for insights throughout my research. Thank you to Drs. Simon de Szoeke, Sandra Yuter, and Paquita Zuidema for providing high quality data for use in my research, as well as to MODIS and to the NRL for providing satellite data and model initialization data, respectively. Thank you to the Naval Research Laboratory for the funding support for my thesis research with award number N00014-11-1-0518. I would like to thank my fellow graduate students Carly Fish and Hannah Chandler, as well as all of the others in other research groups and those who have graduated, for their insights and emotional support they provided when I was stuck. I would like to thank my friend Tom Ball for all of his emotional support during my thesis research. I would like to thank my family for supporting me throughout my entire education and for listening when I needed them to. Finally, I want to

thank my dog, Chipp, who passed away days before my thesis defense due to cancer, for his unconditional love and support throughout my thesis. I will love and miss him forever.

Contents

List of Figures

List of Tables

Chapter 1

Introduction

Marine Boundary Layer (MBL) clouds substantially affect the moisture and energy budgets of the Earth's atmosphere (Krueger et al., 1995; Leach and Raman, 1995). On average, stratocumulus clouds off the western coasts of the continents can cover as much as 34% of the world's oceans (Klein and Hartmann, 1993). These persistent marine clouds greatly increase the Earth's albedo and low cloud feedbacks remain a source of substantial uncertainty in climate models (Bony and Dufresne, 2005; Medeiros et al., 2008), and many of the climatic impacts of MBL clouds are not fully understood (Stocker et al., 2014). On shorter timescales, these clouds produce drizzle and fog which can affect maritime and aviation operations (Mechem and Kogan, 2003).

MBL cloudiness is not characterized by a single cloud type but rather by a continuum of cloud regimes and transitions. Oceanic cloud regimes transition from unbroken stratocumulus near the coast, to open-cell shallow (trade) cumulus further west, followed by cumulus congestus and deep convection in the western tropical oceans (Figure 4 Albrecht et al., 1995; Stevens, 2005, Figure 1). Because many of the processes that occur in clouds (lateral and cloud-top entrainment, microphysical process rates) cannot be accurately resolved in larger-scale models, they need to be

parameterized (McCaa and Bretherton, 2004; Wang et al., 2011). Regional forecast (mesoscale) models have consistently struggled with accurately representing MBL cloud processes.

Rahn and Garreaud (2010a,b) compared output from the Weather Research and Forecasting (WRF) model with observations from VOCALS-REx (VAMOS [Variability of the American Monsoon Systems] Ocean-Cloud-Atmosphere-Land Study - Regional Experiment, hereafter VOCALS, (Mechoso et al., 2014; Wood et al., 2011) and found that the MBL depths were found to vary little along the coast but an east-to-west gradient in sea surface temperature (SST) offshore causes an east-to-west gradient of MBL depths, with the deeper MBL farther west (Rahn and Garreaud, 2010b). Zonal flow in the Southeast Pacific (SEP) is minimal and meridional flow is primarily southerly in the lower troposphere, which can contribute to the northward movement of continental aerosols (seen in satellite data, discussed later) and northwestward propagation of gravity waves off of the Andes. Toniazzo et al. (2011) corroborates the findings of (Rahn and Garreaud, 2010a,b), and also shed light on other MBL properties during VOCALS. For example, they show that a mid-latitude cyclone caused the advection of significant concentrations of aerosols early in November, which were likely the primary source of the marine aerosol load during the first half of our simulations.

Wang et al. (2011) conducted real-time forecast simulations during VOCALS with COAMPS. They not only found consistency in model output when compared to observations from VOCALS, but also found that COAMPS consistently underestimated liquid water path (LWP) of nearshore clouds and nearshore MBL depth. Because synoptic forcing during the VOCALS field campaign was weak, the MBL depth tendency would have been dominated by sub-grid scale turbulence, which would result in more errors in MBL depth during November without proper parameterization (Wang et al., 2011). Error associated with the inability to resolve sub-grid scale microphysics

in mesoscale simulations can be assumed to exist for other boundary-layer and cloud quantities (precipitation, heat and momentum fluxes) that rely on sub-grid scale processes as well. Wang et al. (2011) also show significant improvements to the model output when simulations are run with grid spacings less than or equal to 5 km in the horizontal. Increasing the resolution in their simulations reduced relative error by upwards of 25%-50% for variables like MBL depth or cloud water content (q_c), implying that mesoscale motions, and also sub-grid scale processes, can be extremely important for accurate predictions.

While the ability of numerical weather prediction (NWP) models to represent both cloud systems and the MBL has improved since their inception, single-moment microphysics parameterizations such as (Kessler, 1969) or (Manton and Cotton, 1977) have consistently performed poorly in models. Single-moment parameterizations only account for mixing ratios of the different states of water. For example, the (Kessler, 1969) parameterization fails to accurately represent MBL clouds because of the use of a Heaviside function for autoconversion and fall speed relations tuned for convective environments (Kessler, 1995; Khairoutdinov and Kogan, 2000; Liu et al., 2005). These inabilities to properly represent MBL clouds prompted the development of double-moment parameterizations such as those from Khairoutdinov and Kogan (2000), Liu and Daum (2004), Morrison et al. (2005a,b), and Seifert and Beheng (2006) which sought to alleviate some of the deficiencies of single-moment parameterizations. Double-moment parameterizations account for water mixing ratios like single-moment parameterizations, but also account for the number concentrations of rain drops and cloud drops.

Using a substantial database of aircraft observations, Wood (2005) evaluated microphysical process rates in six different parameterizations by comparing autoconversion and accretion rates calculated by the parameterization formulae with those calculated

directly from the stochastic collection equation (SCE). They found the greatest differences across autoconversion formula; the different formulations of accretion were all quite similar. In addition, they found good agreement between parameterizations and observations for three of the five tested parameterizations, some of which were double-moment parameterizations. Mechem and Kogan (2003) implemented the (Khairoutdinov and Kogan, 2000) parameterization (hereafter KK2000) into COAMPS (Coupled Ocean-Atmosphere Mesoscale Prediction System; Hodur (1997)) and tested it against the COAMPS operational microphysical parameterization (Kessler, 1969; Rutledge and Hobbs, 1983). Unsurprisingly, they found that coarser resolution model runs fail to represent the mesoscale variability that can be found on smaller spatial scales, and that the KK2000 parameterization is more appropriate for marine stratocumulus than the Kessler scheme due to its autoconversion and fall speed formulations. More importantly, they also verified that accounting for the effects of precipitation in models promotes enhanced variability, which the authors interpreted to crudely represent the drizzle-induced transition from stratocumulus to a more decoupled MBL cloud regime.

Observations collected during the VOCALS-REx field campaign give us a prime opportunity to evaluate warm-rain microphysical parameterizations. We conduct multi-day COAMPS simulations for a period during the VOCALS field campaign and perform an extensive evaluation of COAMPS simulations and compare them to the VOCALS observations. In addition, we evaluate how model behavior agrees with accepted observationally based scalings for precipitation rate and coalescence scavenging.

This study has three objectives. First, we will reaffirm the need for double-moment parameterizations for warm-rain microphysical processes. Second, we will show the results from systematic comparisons of parameterizations and observations from both

VOCALS and satellite retrievals. We emphasize that, to the authors' knowledge, this is the first study to compare observed surface drizzle rates from stratocumulus clouds to mesoscale model output drizzle rates. Third, we will use our results to suggest an operational parameterization for warm-rain processes to implement in models. We will also affirm the need for higher resolution simulations, even with parameterizations.

Chapter 2

Methodology

2.1 Model Configuration

For this study, we used the Naval Research Laboratory (NRL) Coupled Ocean-Atmosphere Mesoscale Prediction System (COAMPS version 4, Hodur, 1997). COAMPS employs non-hydrostatic, compressible dynamical equations and parameterizations for subgrid-scale mixing, surface fluxes, microphysics, cumulus convective processes, and radiation. COAMPS integrates acoustically active terms using a mode-splitting technique. The model includes a 1.5-order, 'level 2.5' turbulence closure (Mellor and Yamada, 1982).

COAMPS simulations were conducted for a specific period during VOCALS to promote comparisons with observations. We chose a period from November 12, 2008 through November 16, 2008 because the R/V Ronald H. Brown (hereafter, RHB) spent that time on station (20°S,75°W) collecting observations. We follow Wang et al. (2011) and use the same 45-level vertical grid spacing, which is a trade-off between high resolution and operational computational feasibility (see σ vs. $\Delta\sigma$ plot in Figure 2.1). COAMPS was configured so that the nested model domains centered

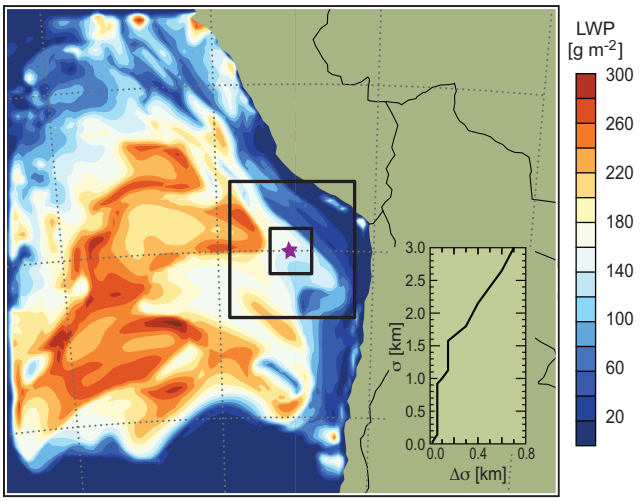

Fig. 2.1 Distribution of grid spacing with height for the vertical grid configuration shown within a contour plot of LWP for the K2013 parameterization at 72hrs into the simulation. Inner bold lines show the second and third nests, respectively The purple star indicates the location of the RHB throughout the simulation period.

on the location of the RHB during this time. We chose to use three nested domains with horizontal gridspacings of 27, 9, and 3 km, and grid sizes of 127×127, 91×91, and 91×91 respectively. Figure 2.1 shows the bounds of each nest, and the purple star at the center represents the location of the RHB during the simulation period. A 24-hour spin-up period, consisting of two model update cycles, was run to properly develop boundary layer thermodynamic and cloud structure. MBL depth was calculated following the method of de Szoeke et al. (2012), which assigns the MBL depth to the level of a relative minimum absolute temperature in each column. In order to prevent erroneous MBL depths, we only considered temperatures in the lower 23 sigma levels (about 1750 m). Rahn and Garreaud (2010a) used a similar method in their study to calculate MBL depth.

The NRL's operational global model NOGAPS (Navy Operational Global Atmospheric Prediction System) provides initial and boundary conditions for COAMPS at

6-hour intervals. The COAMPS initial conditions and update cycles also incorporate additional observations through data assimilation.

2.2 Observations during VOCALS-REx

The VOCALS field campaign was a multi-platform airborne, ship-, and land-based observational campaign intended to sample the Southeast Pacific stratocumulus-topped boundary layer and lower free troposphere (Bretherton et al., 2010; de Szoeke et al., 2010). The campaign lasted from 16 October to 15 November, 2008 and included two research cruises with the RHB. This study uses a subset of data from the second cruise (12–16 November 2008).

We also employed data from the Moderate Resolution Imaging Spectroradiometer (MODIS, Justice et al., 1998) products to asses the degree of horizontal variability of MBL aerosol over the SEP. Unfortunately, the MODIS aerosol products described by Remer et al. (2005) are column-integrated quantities and furthermore assume cloud-free conditions, which is a problem over persistent MBL cloud fields. For these reasons, we follow the methodology of Painemal and Zuidema (2011), which uses MODIS cloud product (Platnick et al., 2003) retrievals to calculate the cloud droplet concentration, N_c [cm^{-3}]. MODIS effective radius (r_e, converted from μm to cm) and optical thickness (τ) products are combined to calculate N_c:

$$N_c = \Gamma^{1/2} \frac{10^{1/2}}{4\pi \rho_w^{1/2} k} \frac{\tau^{1/2}}{r_e^{5/2}} \tag{2.1}$$

which then simplifies to:

$$N_c = 1.4067 \times 10^{-6} \frac{\tau^{1/2}}{r_e^{5/2}}. \tag{2.2}$$

Here, ρ_w is the density of water in kg m^{-3}, k is the cubic ratio between the mean volume radius and the effective radius and is assumed to be constant at 0.8, and

Γ is the approximate adiabatic liquid water content lapse rate. Further discussion can be found in section 3.4 of Painemal and Zuidema (2011). Here we make the assumption that the number of cloud droplets can be considered a proxy for the CCN concentration, and furthermore assume that the variability in N_c is covariant to that of the CCN concentration (Hudson et al., 2010, 2009).

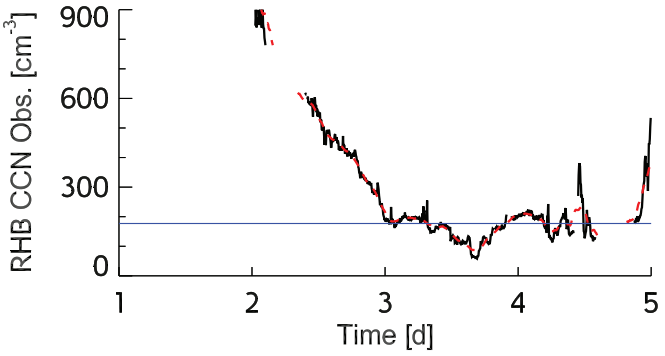

Fig. 2.2 Observed CCN concentrations from the RHB during the simulation period at 0.6 % supersaturation. The blue line indicates the calculated mean (177 cm^{-3}) CCN used to formulate the control CCN concentration initialization. The red line is a moving average of the CCN concentration. Gaps in the data are due to mechanical failure.

Figure 2.2 shows a time series of CCN concentration (S = 0.6%) from the RHB. The period of high CCN concentration early in the simulation is associated with the northwestward movement of a mix of continental and marine aerosol, the concentration of which can be extrapolated from our calculations of N_c in Figure 2.3 and is shown to be anomalously high. We established our control simulation for the CCN concentration sensitivity tests by taking the average of the CCN concentration over the last 2 days of the simulation (177 cm^{-3}) and using that value as the initial CCN concentration. We know that the primary synoptic flow in this region is out of the south, indicating that the anomaly would move north along the continent and dilute to a more homogeneous state (Rahn and Garreaud, 2010a). At all other locations within the outer domain, the distribution of aerosol is largely homogeneous.

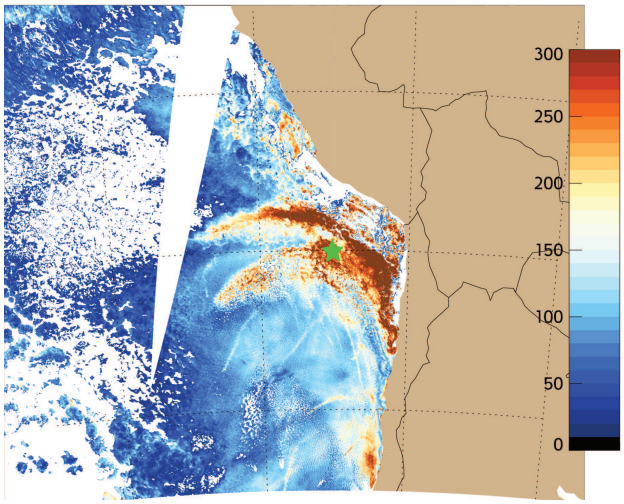

Fig. 2.3 Plots of N_c calculated from MODIS cloud product effective radius and optical thickness following Painemal and Zuidema (2011) at 1km resolution for DOY = 317 at 1510Z. Spatial homogeneity of N_c, and by assuming the covariance of N_c with CCN, the CCN over the majority of the model domain west of (20°S,75°W) where the RHB recorded observations during the simulation period is present upstream. The green star indicate the approximate position of the RHB.

The sensitivity of the parameterizations to CCN concentration is tested by initializing the model with five different spatially homogeneous CCN concentrations. The first is the control simulation with 177 cm^{-3} as described above. Three more simulations were initialized with multiples of the control simulation: 90, 340, and 700 cm^{-3}. Each of these initializations were chosen as being approximately half, double, and 4 times the control simulation CCN initialization. An additional simulation with a CCN initialization of 290 cm^{-3} was employed to conform to the default oceanic CCN concentration in COAMPS.

The remaining observational data used in this study are associated with instruments aboard the RHB, as described in de Szoeke et al. (2010) and de Szoeke et al. (2012). LWP was measured by vertically pointing microwave radiometers as described in Zuidema et al. (2005). Rain rates from the RHB were calculated from radar reflectivity factor sampled from a scanning C-band radar (Burleyson et al., 2013; Comstock et al., 2004). The reflectivity dataset also include reflectivities from radar calibrations of ± 2dBz. We chose to use the C-band radar instead of the W-band cloud radar in order to be able to quantify the spatial variability of precipitation within the VOCALS domain. In addition, laser ceilometers measured the cloud base height, and surface quantities (i.e. temperature, humidity, heat and moisture fluxes) were obtained from instruments mounted on a mast at the front of the ship (de Szoeke et al., 2010).

2.3 Microphysical Parameterizations

The suite of simulations (see Table 2.1) comprises a number of microphysical parameterizations and CCN concentrations. The operational microphysical parameterization using the Kessler warm-rain formulation (Kessler, 1969) is used to establish a baseline control simulation. Subsequent model runs employed the KK2000 microphysics

Table 2.1 List of runs completed with COAMPS. Implemented parameterizations and their variations are listed with the varying CCN concentrations used to initialize COAMPS. Kessler does not account for CCN concentration, or N_c, and thus is separated from the rest of the parameterizations.

Parameterization	CCN Conc. cm^{-3}
Kessler	N/A
KK2000	90
K2013	177
K2013 - No S.C.	290
KK2000 - Threshold	340
K2013 - N.P.	700

parameterization (Khairoutdinov and Kogan, 2000) and a newer microphysical parameterization similar to KK2000 but formulated for shallow cumulus clouds (K2013, Kogan, 2013). Both KK2000 and K2013 are formulated from multivariate non-linear regressions of the droplet spectra from bin-microphysics large-eddy simulations (LES). Refer to Khairoutdinov and Kogan (2000) and Kogan (2013) for complete descriptions of the two parameterizations. Table 2.2 summarizes the equations for the microphysical process rates for each parameterization. The main differences between the Kessler and the KK2000 and K2013 parameterizations are the inclusion of the second moment number concentrations in the equations for the process rates and the assumption of a Marshall-Palmer drop size distribution for the subcloud evaporation process. Because of the method of formulation for KK2000 and K2013, both parameterizations are very similar. However, their main differences are in the exponents of the non-linear regressions that make up the process rates, particularly an approximately double dependence on N_c in the the autoconversion rate for K2013 which makes the K2013

parameterization more sensitive to the number concentration of cloud droplets.

K2013 also includes a term that represents the self-collection of precipitation droplets that KK2000 does not account for. To test the importance of including this self-collection term in warm-rain parameterizations, we performed additional simulations of K2013 omitting the self-collection term. Another test of the internal microphysics of the model was performed by adding a suite of simulations with the addition of a critical droplet radius threshold of Liu and Daum (2004) to the KK2000 autoconversion rate following Mechem and Kogan (2008) employed to address spurious overestimation of precipitation at large CCN concentrations. Our final suite of simulations attempt to capture the overestimation of precipitation in mesoscale models by removing coalescence processing of cloud droplets (the depletion of cloud droplet concentration accompanying the coalescence process) due to autoconversion and accretion.

Table 2.2 Details of the equations that comprise each parameterization used in the study. (Kessler, 1969) is the operational microphysics for COAMPS V4.

	Kessler	KK2000	K2013
Accretion	$\left(\frac{\partial q_r}{\partial t}\right)_{accr} = 6.96 \times 10^{-4} E N_0^{1/8} q_c q_r^{7/8}$	$\left(\frac{\partial q_r}{\partial t}\right)_{accr} = 67 \left(q_c q_r\right)^{1.15}$	$\left(\frac{\partial q_r}{\partial t}\right)_{accr} = 8.53 q_c^{1.05} q_r^{0.98}$
Autoconversion	$\left(\frac{\partial q_r}{\partial t}\right)_{auto} = k_1 \left(q_c - a\right)$ $k_1 = 10^{-3} s^{-1}, 0.5 < a < 1.0 g q_c^{-3}$	$\left(\frac{\partial q_r}{\partial t}\right)_{auto} = 1350.0 q_c^{2.47} N_c^{-1.79}$	$\left(\frac{\partial q_r}{\partial t}\right)_{auto} = \left(7.98 \times 10^{10}\right) q_c^{4.22} N_c^{-3.01}$
Fall Speed	$V = -38.3 N_0^{-1/8} q_r^{1/8}$	$V_{N_r} = 0.007 r_{vr} - 0.1$ $V_{q_r} = 0.012 r_{vr} - 0.2$	$V_{N_r} = 0.385 r_{vr} + 5.76$ $V_{q_r} = 2.4 r_{vr} - 62.0$
Evaporation	$\left(\frac{\partial q_r}{\partial t}\right)_{evap} = 1.93 \times 10^{-6} N_0^{7/20} q_c q_r^{13/20}$	$\left(\frac{\partial q_r}{\partial t}\right)_{cond} = 3 C_{evap} G\left(T, p\right) \left(\frac{4\pi\rho_w}{3\rho_a}\right) q_r^{1/3} N_r^{2/3} S$	$\left(\frac{\partial q_r}{\partial t}\right)_{cond} = \frac{4\pi G\left(T, p\right) \rho_w}{rho_a} S N_r \overline{r_r}$
Self-Collection	N/A	N/A	$\left(\frac{\partial q_r}{\partial t}\right)_{scol} = 205 q_r^{1.55} N_r^{0.60}$

Chapter 3

Results

Here we present simulation results and compare them with RHB observations. We also evaluate the internal consistency of model microphysical processes by exploring how well simulated cloud properties adhere to observationally derived scalings for precipitation rate and coalescence processing.

3.1 Model Output

Figure 3.1 shows time-height contour plots of cloud water mixing ratio (q_c), rain water mixing ratio (q_r), and liquid water potential temperature (θ_l) for each parameterization on the inner mesh (3 km) of the control simulation (177 cm^{-3}). Upon first glance, the most prevalent feature is the coincident stratification of the boundary layer and overall increase in q_r and decrease in q_c at the start of day 3 for all except the Kessler simulation. This stratification of the boundary layer is the result of the warming of the upper boundary layer and the cooling of the surface layer. Warming of the cloud layer is assumed to be due to the effects of the drizzle-induced asymmetry in the MBL circulation (Stevens et al., 1998). The cooling at the surface is due

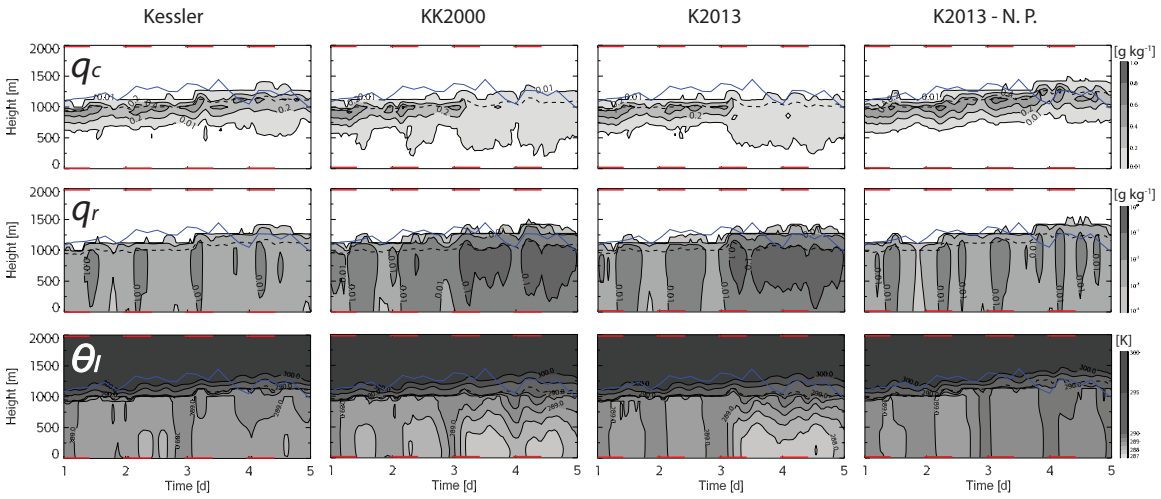

Fig. 3.1 Time-height cross-sections of q_c, q_r, and θ_l from the inner mesh for each parameterization during the control simulation (CCN = 177 cm^{-3}). Red lines above the plots indicate night time for reference to the diurnal cycle. The blue line indicates the observed MBL depth.

simply to evaporation of drizzle. This sudden change in the model fields at the start of day 3 is coincident with forecast divergence in the model, but we assert that this change is not associated with forecast divergence. Rather, we hypothesize that precipitation efficiency is increasing with time throughout the simulation, which causes the higher precipitation rates and depletion of cloud after day 3. The stabilization of the boundary layer due to the increased precipitation as described above creates a "cap" that prevents moisture fluxes from reaching the cloud layer to restore cloud in the boundary layer. In this sense, the cloud can be seen as a residual of the balance between precipitation processes and moisture fluxes.

Figure 3.1 also shows that the model exhibits a diurnal cycle of precipitation and θ_l, particularly evident early in the simulation. The timing of the precipitation onset is consistently just around local sunset, consistent with the results for the western portion of the VOCALS domain in Burleyson et al. (2013). The right-most column of Figure 3.1 representing the "no processing" (K2013-N.P.) simulation shows very

different characteristics than the other simulations. First, it shows a very robust diurnal cycle, with the cloud water mixing ratio increasing overnight and does not exhibit the same sudden decrease in cloud water that the other simulations do. Furthermore - and perhaps most importantly - the K2013-N.P. simulation does not exhibit the same increase in rain water mixing ratio after day three of the simulation, which in turn also keeps the boundary layer more well-mixed throughout the simulation. This is because the low rain rates keep the evaporative cooling at the surface much lower, inhibiting large degrees of stabilization in the lower boundary layer.

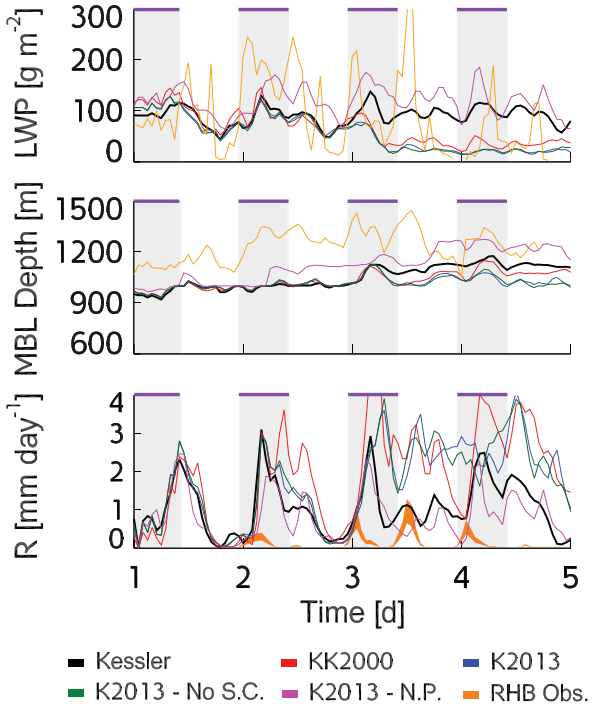

Fig. 3.2 Time series of hourly averaged LWP, MBL, and R from the inner nest for each parameterization during the control simulation (CCN = 177 cm^{-3}), and observations from RHB. Purple lines above the plot and transparent bars indicate night time. Observed R includes ± 2 dBz radar calibration values and are banded into the observed values.

Figure 3.2 shows time series of simulated LWP, MBL depth, and precipitation rate, all compared with RHB observations for the control simulation. Simulation

statistics are provided by Table 3.1, which shows the simulation mean values for LWP, MBL depth, and precipitation rate. Figure 3.3 visualizes the Table 3.1 data for easier comparison between parameterizations and CCN initializations. All simulations underestimate LWP relative to that observed by the RHB. The simulation mean LWP increases as the CCN concentration increases (see Table 3.1 and Figure 3.3), which indicates suppression of precipitation by large CCN concentrations. The larger peaks in model LWP tend to occur coincidentally with the high precipitation rates overnight, and are associated with the diurnal cycle just after sunset, contrary to the results of Burleyson et al. (2013) for the eastern portion of the VOCALS domain. In addition, Burleyson et al. (2013) found that drizzle was present throughout the day as well, which we found to be the case in our model simulations. One source of discrepancy between the LWP from the RHB and the model is due to the RHB LWP being a point measurement taken from microwave radiometers, whereas the model LWP is a domain-average quantity. The largest model LWP comes from the K2013-N.P. simulations, and is due to the smaller rain rates, leaving more liquid water in the atmosphere as cloud.

The middle panel of Figure 3.2 shows the hourly averaged MBL depth for the simulation and exhibits the same overall model underestimation when compared to observed values. The underestimation of the MBL depth is a persistent problem in both mesoscale and climate models (Wang et al., 2011; Wyant et al., 2015). The MBL depth is affected by CCN concentration through stabilization of the MBL by precipitation evaporation, which leads to a reduction of cloud-top entrainment. Combined, these effects make the MBL more shallow and overall stratify the boundary layer, as seen in the θ_l time-height cross-sections in Figure 3.1. The only quantity that doesn't follow the same underestimation pattern is the precipitation rate. Furthermore, our K2013-N.P. simulations show a higher MBL depth than the other simulations throughout

the majority of the simulation period. This is likely because, as discussed above, not allowing for droplet processing due to autoconversion and accretion increases the number of cloud droplets and lowers the rain rates, which in turn deepens the MBL because of the decreased drizzle-induced evaporative cooling at the surface. For all CCN concentrations, the precipitation rate is typically much greater than the observed values, sometimes as much as 4 times as large. The K2013-N.P. simulations have much lower rain rates than the other parameterizations and exhibit most of the diurnal characteristics as the other simulations.

Table 3.1 and Figure 3.3 also emphasize how much the model output can diverge from the observations. Lower CCN concentrations result in LWP values of at least 50 g m^{-2} lower than the observations (likely because of the MBL being shallow) and values associated with higher CCN concentrations will actually surpass the observational values by approximately 30 g m^{-2}. Similarly, all of the parameterizations underestimate the observed, average MBL depth by just under 150 meters. Model precipitation rates suffer from significant overestimation, as discussed, by approximately 2 orders of magnitude for low CCN simulations.

In addition to the parameterization suite shown in Figure 3.2, Table 3.1 and Figure 3.3 include results from an additional simulation series, where the critical radius threshold from Liu and Daum (2004), as simplified by Wood (2005), is imposed on the autoconversion term from KK2000 following Mechem and Kogan (2008). The motivation for these simulations is to address the overestimation of precipitation in a physically meaningful way. Imposing this threshold on the autoconversion process, suppresses the precipitation rates for simulations initialized with higher CCN concentrations. The rain rates in the KK2000-threshold simulations approach the observed rain rates (Table 3.1, Figure 3.3). In addition, LWP (and MBL depth) nevertheless remain anomalously high (low) relative to the RHB observations. This result suggests

Table 3.1 Simulation mean LWP [g m^{-2}] (a), MBL depth[m] (b), and precipitation rates [mm day^{-1}] (c) for all simulations and all parameterizations. The KK2000 - Threshold run includes the addition of a critical radius threshold for autoconversion following (Liu and Daum, 2004). The observational means are given as a single value covering the range of CCN values observed during VOCALS. The Kessler mean is given as a single value because it does not include prognostics for CCN concentration and N_c.

	CCN Conc.	RHB	Kessler	KK2000	K2013	K2013-No S.C.	KK2000-Thresh.	K2013-N.P.
a)	90			39.62	29.90	26.66	188.30	85.16
	177			62.37	53.57	52.81	191.81	104.48
LWP	290	92.35	80.11	83.71	80.96	79.39	187.77	120.64
	340			89.79	91.05	90.25	193.78	126.41
	700			122.85	123.05	126.45	194.75	137.56
b)	90			1022.95	949.57	966.47	1090.09	1053.85
	177			984.52	971.94	970.44	1090.03	1059.08
z_i	290	1217.27	999.17	1002.02	1003.98	1003.46	1080.26	1064.12
	340			1042.74	1043.74	1009.96	1089.62	1067.42
	700			1073.37	1022.70	1069.56	1090.15	1071.49
c)	90			1.923	1.857	1.867	0.069	0.935
	177			1.518	1.374	1.378	0.0246	0.682
R	290	0.074	0.859	0.964	0.80	0.842	0.015	0.501
	340			1.104	0.864	0.699	0.0082	0.483
	700			0.587	0.353	0.505	0.0044	0.376

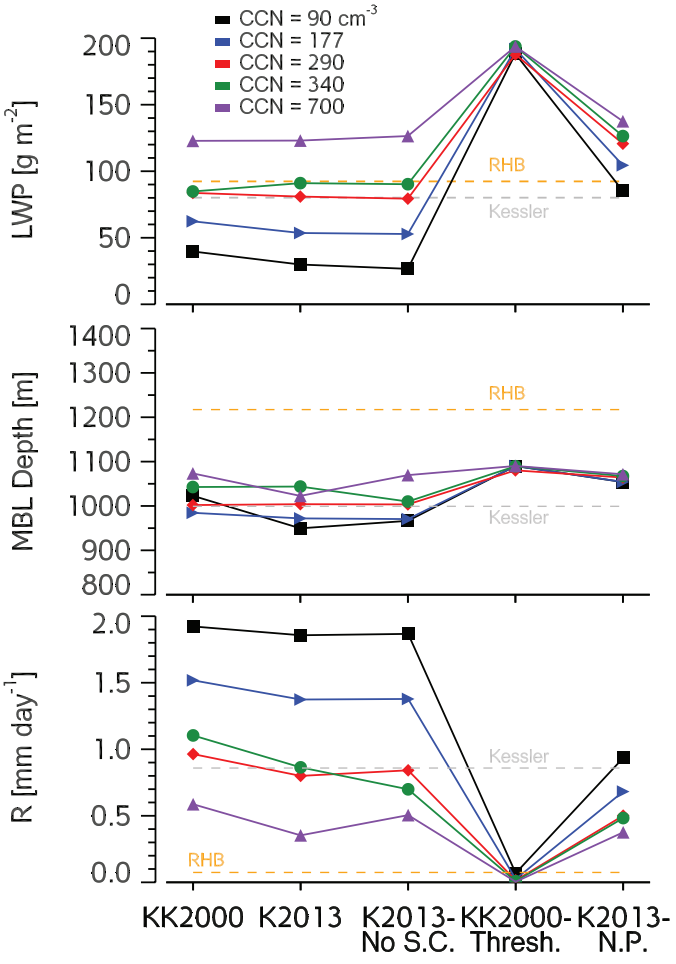

Fig. 3.3 Simulation means of LWP, MBL depth, and R for all parameterizations and all CCN initializations. The Kessler simulation mean is indicated by the gray, dashed line. The observations from the RHB are represented by the orange, dashed line.

that although the critical radius threshold reduces precipitation, imposing a critical radius threshold may not be internally microphysically consistent. Further discussion of microphysical consistency will be done in the next section.

In order to investigate the statistical variability of the model output we constructed normalized probability density functions (PDFs) of LWP (row 1), MBL depth (row 2) and R (row 3) from three different CCN initializations and the RHB observations (see Figure 3.4). The PDFs were calculated over a radius of 60 km to correspond to the sampling area of the RHB C-band radar (centered at (20°S,75°W). The PDF of the Kessler LWP differs most from the PDF of the observations, including none of the larger LWP values in the tail of the observed PDF. As CCN concentration increases, the PDFs of LWP for the tested parameterizations shift from a negative exponential distribution to a more Gaussian distribution, and there are greater differences from the observed LWP PDF. Furthermore, the shapes of each respective parameterization's PDF also begin to diverge from each other with the increase of CCN concentration. The PDF of LWP from the K2013-N.P. simulation does not exhibit the same negative exponential distribution as the other simulations, but rather remains relatively Gaussian, and widens as the CCN concentration increases. The narrowness and similarity of the MBL depth distributions in the CCN = 177 and 340 cm^{-3} simulations suggest that CCN plays little role in modulating MBL depth. Only for the cleaner case (CCN = 90 cm^{-3}) do modest differences in MBL depth begin to appear. We also acknowledge the possibility that COAMPS may not be adequately representing the diurnal upsidence wave described in Garreaud and Muñoz (2004). Whether or not this is the case is beyond the scope of this study. Furthermore, we hypothesize that the coarse horizontal grid spacing of our simulations results in a lack of resolved internal variability including aspects of open and closed cells. The PDFs of both the model and observed precipitation rates are negative exponential

distributions. The model PDFs do not appear to change much across the different CCN concentrations, but the CCN = 177 cm^{-3} simulation appears to have the most agreement between the parameterizations, particularly the K2013 and K2013–No S.C. simulations.

Figure 3.5 casts the model output from all simulations (except the KK2000-threshold) in N_c–LWP parameter space. The data points are color-coded both by parameterization (Figure 3.5a) and by the rain rate (Figure 3.5b). For each parameterization we include simulation mean N_c and LWP values that encompass all sensitivity simulations through time. Since the Kessler microphysics neglects N_c, we include a band corresponding to the range of hourly domain-averaged LWP values for the Kessler simulation in Figure 3.5b in order to asses the accuracy of Kessler microphysics relative to the other parameterizations within the parameter space. The distribution of the data within this parameter space is consistent with higher precipitation rates accompanying lower CCN concentrations and larger LWP, and smaller precipitation rates accompanying with higher CCN concentrations. While it is well known that the highest rain rates will occur in cleaner cases, the model exhibits a sharp increase in precipitation range at $N_c \approx 30$ cm^{-3}, where precipitation rates are nearly 1 mm day^{-1} higher than those for N_c greater than 30 cm^{-3}. Furthermore, variability in LWP for a given cloud droplet concentration increases as the CCN concentration increases. The location of the mean N_c and LWP from implemented parameterizations and the observations indicate that the majority of the observations correspond to relatively high CCN concentrations which is corroborated from Figure 2.2, specifically from early in the simulation. In addition, we speculate that the low mean values of N_c may be the result of precipitation scavenging of droplets and the lack of a suitable source of CCN in the model (Mechem et al., 2006). Our results from the K2013-N.P. simulation support this hypothesis.

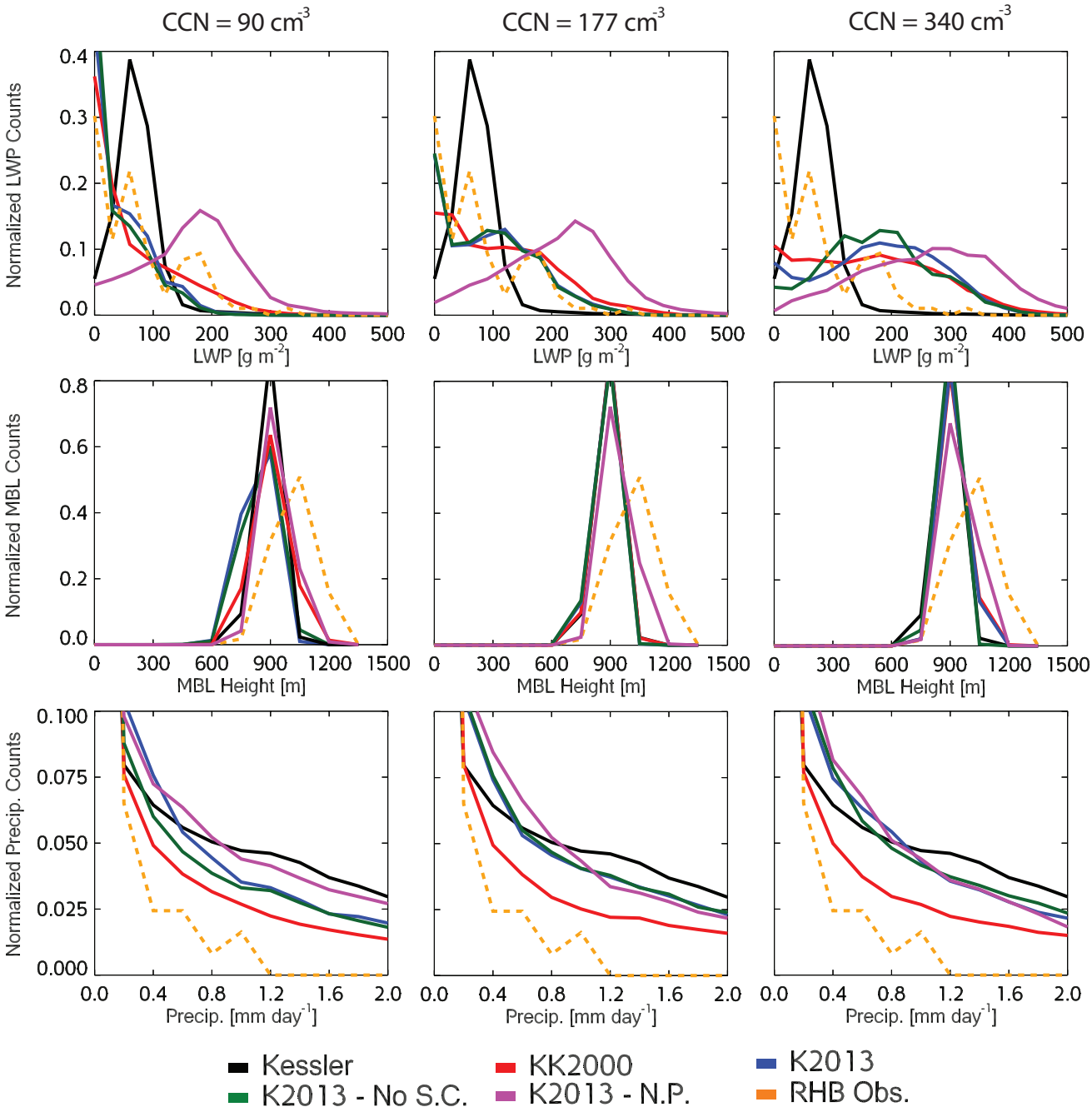

Fig. 3.4 Probability density functions calculated over the volume of the C-band radar (60km radius) aboard the RHB for LWP, MBL, and R for the control simulation (CCN = 177 cm^{-3}) as well as half and double the control CCN concentration. PDFs of observations are dashed, orange lines.

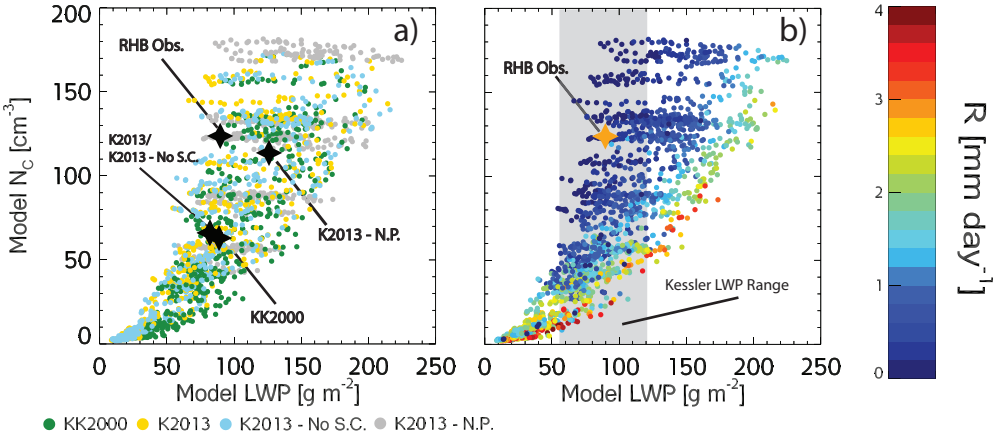

Fig. 3.5 Scatterplots of N_c versus LWP from the inner nest for all parameterizations and all CCN concentrations. The left plot shows the distribution of points by parameterization and the right plot shows the distribution of points by precipitation rate. The mean N_c and LWP for each parameterization are plotted in the left plot. In lieu of scatter points for the Kessler simulations, we indicate the range of hourly domain-averaged LWP values from the Kessler simulation.

3.2 Model Scalings and Microphysical Behavior

Here we explore how well the simulation results adhere to observationally and theoretically scalings, which we interpret as a measure of microphysical consistency in the model. In this section, we use the term "microphysically consistent" to indicate that the microphysical aspects of the model seem to be working, indicating that model error likely has sources other than the model microphysics. Our analysis in this section is similar to the methodology of Geoffroy et al. (2008), where we compare the model output to scalings we assume to be true.

Figure 3.6 shows simulation precipitation rates plotted as a function of the scalings from Comstock et al. (2004) and van Zanten et al. (2005). The adapted equation from Comstock et al. (2004) is

$$R = 0.3744\,(LWP/N_c)^{1.75}\,, \tag{3.1}$$

where R is the precipitation rate in mm day^{-1}, LWP has units of g cm^{-2}, and N_c has units of cm^{-3}. The precipitation scaling from van Zanten et al. (2005) depends on the the cloud thickness, h, instead of LWP and has the form

$$R = 2 \times 10^{-6} \left(h^3 / N_c \right). \tag{3.2}$$

Here the units for R and N_c are the same as in Equation 3.1 and h has units of meters. These scalings were also created for the RHB observations, and are shown in the righthand column of Figure 3.6. In Equation 3.2 the leading coefficient incorporates the factor for the unit change into the original coefficient. Our analyses here do not include results from the Kessler simulation because the Kessler formulation does not include a prognostic for droplet concentration.

The observational scalings hold relatively well for the model output, however, we see that the model output scalings have a wider range of precipitation rates than the observations in Comstock et al. (2004, Figure 10) and van Zanten et al. (2005, Figure 7a). Geoffroy et al. (2008) uses LES simulations to analyze the same scalings, and when compared to their results, our model scalings for precipitation match theirs very well. The majority of the rain rates for both studies lie between 0.1 and 1.0 mm day^{-1}. The scaling values for the Comstock et al. (2004) lie between $(LWP/N_c)^{1.75} = 0.5$ and 100.0 g m^{-2} cm^3 and the scaling values for the van Zanten et al. (2005) study lie between $h^3/N_c = 10^5$ and 10^7 m^3 cm^3. Our results from the K2013-N.P. simulation also follow the scalings with the rain rates being substantially lower than the other simulations as discussed above. The precipitation scalings from Geoffroy et al. (2008) do not, however, contain the same scale break as our results, seen in Figures 3.6a and 3.6c at approximately $(LWP/N_c)^{1.75} = 5.0$ g m^{-2} cm^3 and $h^3/N_c = 5.0 \times 10^5$ m^3 cm^3, respectively. One hypothesis we have to address this is that the observational scalings were developed using cloud-base rain rates, whereas our model output and observations

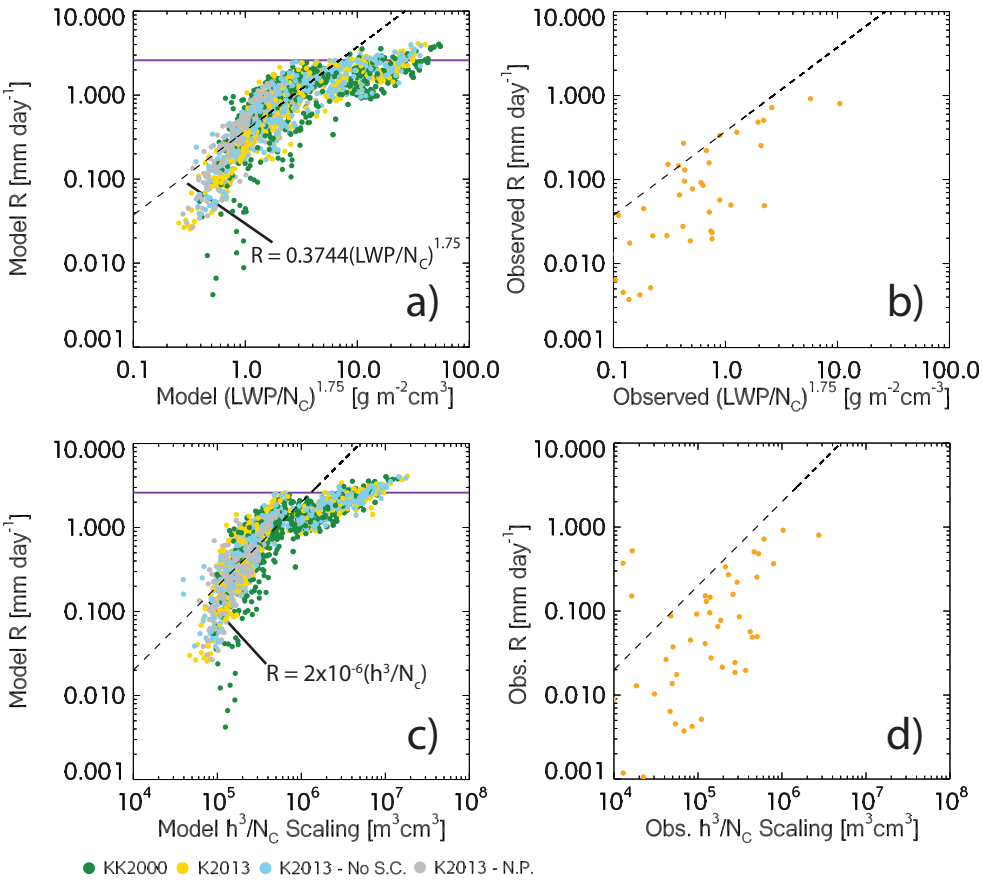

Fig. 3.6 Precipitation scalings for the inner nest and observations from RHB. The top row scalings follow (Comstock et al., 2004) and the bottom row scalings follow (van Zanten et al., 2005). The equations for each line have been adapted from both previous studies to the units used in this study. The solid purple line indicates a rain rate calculated from the equivalent mean latent heat flux from all simulations.

are all surface (or near-surface) precipitation measurements. We hypothesize that using cloud-base instead of surface rain rates would increase the rain rates for the lower $(LWP/N_c)^{1.75}$ and h^3/N_c scalings because the drizzle rates are highest at cloud base and thus the currently prominent scale break would no longer be present. As an alternative, we hypothesize that the scale break might also arise from a simple water budget constraint. We have included a purple line at $R = 2.6$ mm day^{-1} on Figure 3.6 that corresponds to the mean latent heat flux for all simulations (76.86 W

m^{-2}). The idea here is that you can't rain out more water than is evaporated into the boundary layer, which makes the latent heat flux a limiting factor on rain rates in these simulations. Furthermore, this latent heat flux limiting indicates that the scale break is not entirely physical. Geoffroy et al. (2008) found significant overestimation of model precipitation rates as we did, which implies that there may be issues within models than we currently do not understand and that will need to be addressed. In addition, the K2013-N.P. simulation does not exhibit the scale break that the other simulations do, likely because the rain rates are not as high as they are in the other simulations and thus does not depend on the hypothesized latent heat flux limiting.

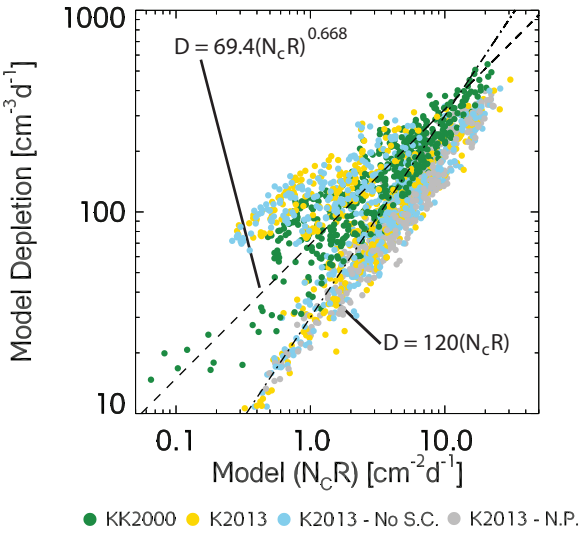

Fig. 3.7 Model depletion of CCN following (Wood, 2006), whose scaling equation has been adapted to $D = 120\,(N_c R)$. The other equation is from (Mechem et al., 2006) which also used the method of (Wood, 2006) but found a slightly different set of parameters for CCN depletion.

In addition to scalings for precipitation rate, we also explore scalings for coalescence processing for the depletion rate of cloud droplets from coalescence. Figure 3.7 shows coalescence processing rates from all simulations, along with two scalings found in the literature (Mechem et al., 2006; Wood, 2006). Figure 3.7 replicates the scalings in two specific studies, each with their own regression equations for CCN depletion. Wood

(2006) developed a theoretically based expression for coalescence processing, given as

$$D = 120\,(N_c R)\,. \tag{3.3}$$

Mechem et al. (2006) found a formulation based on highly idealized COAMPS simulations, given as

$$D = 69.4\,(N_c R)^{0.668}\,. \tag{3.4}$$

In both equations, N_c is the number concentration of cloud droplets in cm^{-3}, R is the precipitation rate in mm day^{-1}, and D is the depletion rate of cloud droplets in cm^{-3} day^{-1}. From Figure 3.7, it is clear that the KK2000 parameterization holds best to both previous studies' depletion scalings across the range of N_c and R values based on how closely the KK2000 data points cluster around the scaling regression lines. It is important to note, however, that despite the somewhat wider spread of data from K2013 and K2013–No S.C., the output from all simulations hold very closely to both of the coalescence scavenging scalings found in Wood (2006) and Mechem et al. (2006). The results from the K2013-N.P. simulation follow the scaling from Wood (2006) very closely and does not exhibit the same spread in the data as the other simulations because the total particle concentration ($N_c + N_{CCN}$) is constrained. We could not create a similar plot for the RHB observations because the N_c depletion rate was not observationally available from the VOCALS-REx datasets.

Figure 3.8 shows the previous scalings but over the outer nest (with 27 km grid spacing). The most obvious results from evaluating scalings on the outer nest is the significantly wider distribution of data points and the complete disagreement with the observational scalings. This indicates that lower resolution simulations do not remain microphysically consistent and the results from those simulations are not as robust. Figure 3.9 shows the same scalings discussed above for the middle (9 km) nest. These results confirm that model horizontal resolution remains acutely important to

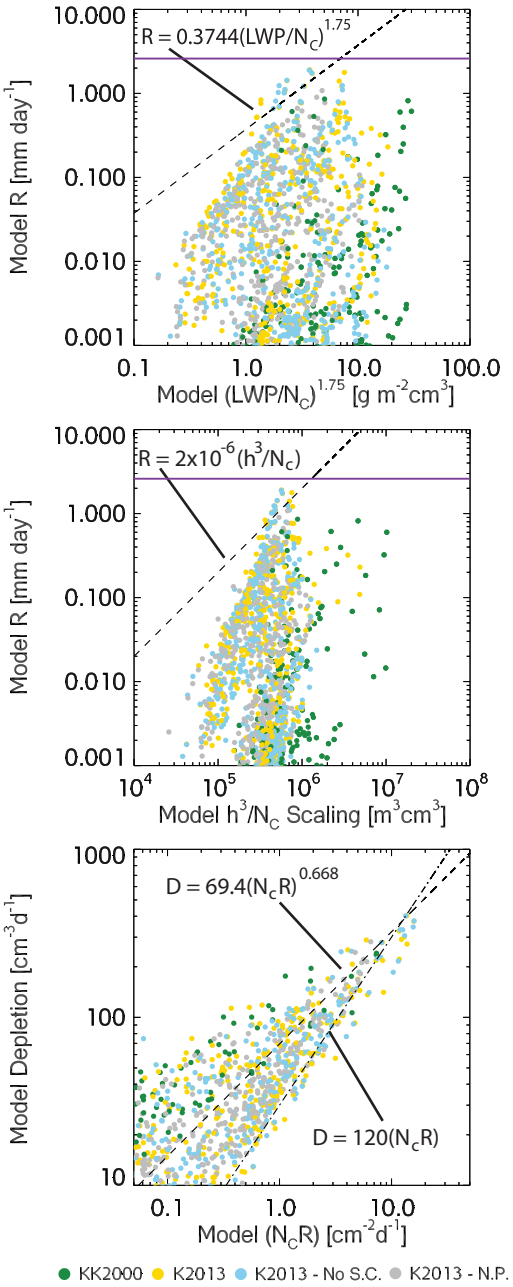

Fig. 3.8 Scalings from Figures 3.6 and 3.7 but for the outer nest.

microphysical consistency. The spread of the data in the precipitation scalings show a similar behavior to the finest mesh simulation in Figure 3.6, which indicates that the second nest of the suite of simulations (9 km grid spacing) are microphysically consistent. The results for the N_c depletion rates adhere to the scalings of Mechem et al. (2006) and Wood (2006), further indicating internal microphysical consistency within the implemented parameterizations.

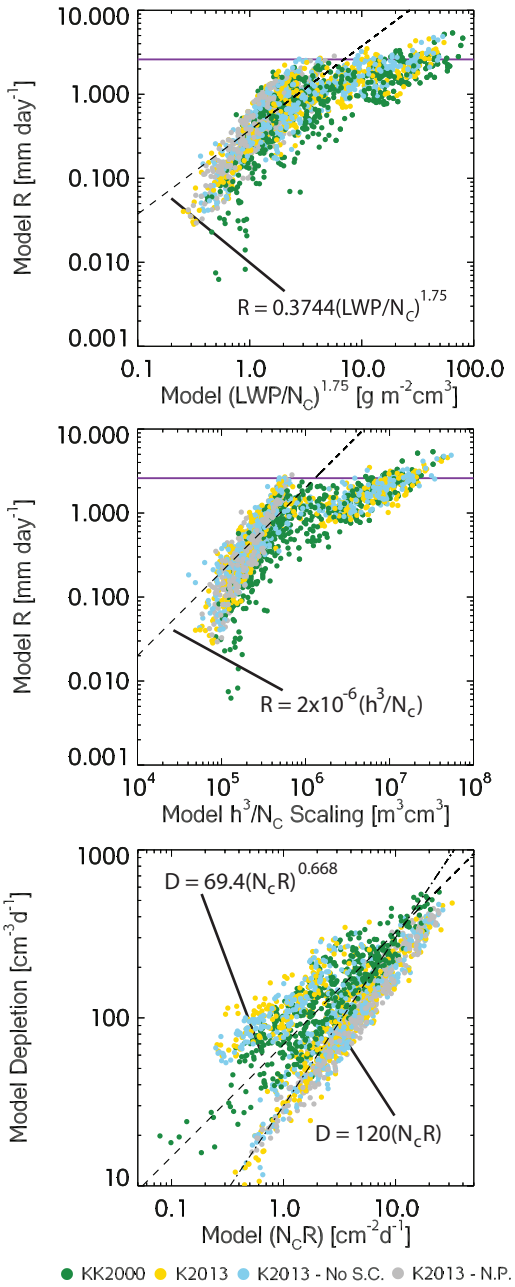

Fig. 3.9 Scalings from Figures 3.6 and 3.7 but for the middle (second) nest.

Chapter 4

Discussion and Conclusions

4.1 Forecast Analysis

The suite of simulations show that the KK2000 and K2013 parameterizations do not appear to operate in significantly different ways. The similarity of the results between KK2000 and the K2013/K2013-No S.C. simulations is expected as the later was shown to perform very closely to KK2000 in the case of MBL stratocumulus. This makes sense given the multivariate linear regression method of formulation for each parameterization (Khairoutdinov and Kogan, 2000; Kogan, 2013), even though the individual formulations themselves have significant differences in process rates (see Table 2.2). The slight differences may be due to somewhat thicker VOCALS stratocumulus compared to thinner ASTEX (Atlantic Stratocumulus Transition Experiment, Albrecht et al., 1995) stratocumulus tested in Kogan (2013). Our results for primary boundary layer quantities (LWP, MBL depth, and R) show very little variability from the other newly implemented parameterizations in Figure 3.4. Figure 3.2 shows that the parameterizations only show large amounts of disagreement after 2 full days of simulation. Operationally speaking, this kind of disagreement from observations is

relatively normal for model forecasts as time increases. To avoid these errors, models are initialized with data assimilation schemes and contain more update cycles. Some of these errors appear to be reduced when $N_{CCN} + N_c$ is held constant, implying the importance of parameterizing a source term for CCN.

Current formulations of the newly implemented parameterizations all perform very similarly. However, K2013 shows promise for being the best choice (of the three implemented parameterizations) for primary use in mesoscale models due to its generality and ability to perform in both stratocumulus and trade cumulus cloud regimes, making it applicable to a wider variety of simulations (Kogan, 2013). Using the no self-collection variant of K2013 would also be a suitable choice for mesoscale simulations in cloud systems like those we have evaluated. That said, there is still a significant amount of divergence from observations associated with all parameterizations (see Table 3.1 and Figure 3.3). As always, the horizontal and vertical resolution play a large role in accurately simulating the MBL depth, and with increased computational infrastructure, forecast error will likely decrease significantly (Wang et al., 2011; Wyant et al., 2015). However, when we consider the present, much of the bias causing this divergence from observations is likely associated with errors in the boundary-layer parameterization that need to be addressed (Grenier and Bretherton, 2001). We assert this because of the general model agreement on LWP and MBL depth from each parameterization and the lack of replenishment of CCNs due to advection and mixing (see Figure 3.5), while still having negative model bias for the LWP and MBL depth. Any remaining model error is likely associated with errors in microphysics parameterizations, and would likely be mitigated with the addition of a parameterization that accounts for sub-grid scale microphysical processes, such as Kogan and Mechem (2014).

4.2 Microphysical Consistency

The scalings produced by the inner simulation mesh in Figures 3.6 and 3.7 indicate that the model microphysics is consistent with what has been found to be true for stratocumulus clouds in observational studies (Comstock et al., 2004; Mechem et al., 2006; van Zanten et al., 2005; Wood, 2006). These findings are consistent with Geoffroy et al. (2008), whose LES simulations closely resemble the observational scalings evaluated from three different observational studies. Because they used LES simulations, they explicitly resolve the process rates instead of parameterizing them, which likely increases the adherence of their model output to the observational scalings.

It is important to note that in order for these parameterizations to maintain microphysical consistency, the models must be run at relatively high resolutions (approximately a 10 km grid spacing or lower), which is based on scaling results from the second mesh (Figure 3.9). Running at higher resolutions will cause some amount of delay in regular output due to computational constraints, but the dramatic shift in model accuracy from 27 to 10 km may justify higher resolution mesoscale simulations. In addition, these parameterizations do not remain microphysically consistent when run at larger grid spacings, further justifying higher resolution simulations. The 27 km results in Figure 3.8 shows this quite well. As discussed earlier, K2013 and K2013 without self-collection have the best adherence to the scalings at low resolution and should be used should low resolution simulations be necessary, but it is important to note that the K2013 simulations have a higher dependence on N_c suggesting a greater sensitivity to N_c. This effect, however, is not reflected in our simulations.

4.3 Final Thoughts

We have presented the results from a suite of COAMPS simulations that test various warm-rain microphysical parameterizations during 12–16 November of VOCALS-REx in 2008, as well as systematic comparisons with observations from both MODIS and VOCALS. While all of the implemented parameterizations perform well and would be suitable for mesoscale simulations, our results suggest that the K2013 parameterization is the best choice for implementation in mesoscale models because it remains internally, microphysically consistent and because it performs well in multiple cloud regimes. Implementing the Liu and Daum (2004) autoconversion threshold as an addition to KK2000 (as in Mechem and Kogan (2008)) is not appropriate. Although the threshold does suppress the precipitation rates, it is not a physically based solution as the LWP is too high and remains constant across all CCN initializations. Furthermore, the MBL depth has little to no variability for the simplified Liu and Daum (2004) implementation (see Table 3.1 and Figure 3.3).

We encourage the following when running mesoscale simulations. First, ensure to run models with at least 10km grid spacing to ensure the proper microphysical consistency. If computational resources or time can be afforded, grid spacings smaller than 10 km would be preferable. Second, based on its generality, we suggest the use of the Kogan (2013) warm-rain microphysics parameterization because of its applicability to both stratocumulus cloud sheets and trade cumulus regimes. However, the KK2000 parameterization performs equally as well over the VOCALS period studied here. Simulations in the trade cumulus regime may better reap the advantages of the K2013 parameterization. We speculate that including other methods of parameterizing sub-grid scale microphysical processes, such as the method found in Kogan and Mechem (2014) would improve model output as well.

Bibliography

Albrecht, B. A., C. S. Bretherton, D. Johnson, W. H. Schubert, and A. S. Frisch, 1995: The atlantic statocumulus experiment — ASTEX. *Bull. Amer. Meteor. Soc.*, **76**, 889–904.

Bony, S. and J. Dufresne, 2005: Marine boundary layer clouds at the heart of tropical cloud feedback uncertainties in climate models. *Geophys. Res. Lett.*, **32**, L20 806, doi:10.1029/2005GL023851.

Bretherton, C. S., R. Wood, R. C. George, D. Leon, G. Allen, and X. Zheng, 2010: Southeast pacific stratocumulus clouds, precipitation, and boundary layer structure sampled along 20/degree s during vocals-rex. *Atmos. Chem. Phys.*, **10**, 10 639–10 654, doi:10.5194/acp-10-10639-2010.

Burleyson, C. D., S. P. deSzoeke, S. E. Yuter, M. Wilbanks, and W. A. Brewer, 2013: Ship=based observations of the diurnal cycle of southeast pacific marine stratocumulus clouds and precipitation. *J. Atmos. Sci.*, **70**, 3876–3894, doi:10.1175/JAS-D-13-01.1.

Comstock, K. K., R. Wood, S. E. Yuter, and C. S. Bretherton, 2004: Reflectivity and rain rate in and below drizzling stratocumulus. *Q. J. R. Meteorol. Soc.*, **130**, 2891–2918.

de Szoeke, S. P., S. Yuter, D. Mechem, C. W. Fairall, C. D. Burleyson, and P. Zuidema, 2012: Observations of stratocumulus clouds and their effect on the eastern pacific surface heat budget along 20. *J. Climate*, 8542–8567, doi:10.1175/jcli-d-11-00618.1.

de Szoeke, S. P., S. E. Yuter, P. Zuidema, C. W. Fairall, and W. A. Brewer, 2010: Ship-based observation of drizzling stratocumulus clouds from EPIC to VOCALS. *CLIVAR*, **39**, 11–13.

Garreaud, R. D. and R. Muñoz, 2004: The diurnal cycle in circulation and cloudiness over the subtropical South Pacific: A modeling study. *J. Climate*, **17**, 1699–1710.

Geoffroy, O., J.-L. Brenguier, and I. Sandu, 2008: Relationship between drizzle rate, liquid water path, and droplet concentration at the scale of a stratocumulus cloud system. *Atmos. Chem. Phys.*, **8**, 4641–4654.

Grenier, H. and C. S. Bretherton, 2001: A moist pbl parameterization for large–scale models and its application to subtropical cloud–topped marine boundary layers. *Mon. Wea. Rev.*, **120**, 357–377.

Hodur, R., 1997: The naval research laboratory's coupled ocean/atmosphere mesoscale prediction system (coamps). *Mon. Wea. Rev.*, **125**, 1414–1430.

Hudson, J. G., S. Noble, and V. Jha, 2010: Stratus cloud supersaturations. *Geophy. Res. Lett.*, **37**, doi:10.1029/2010GL045197.

Hudson, J. G., S. Noble, V. Jha, and S. Mishra, 2009: Correlations of small cumuli droplet and drizzle drop concentrations with cloud condenstaion nuclei concentrations. *J. Geophys. Res.*, **114**, doi:10.1029/2008JD010581.

Justice, C. O., et al., 1998: The moderate resolution imaging spectroradiometer

(modis): Land remote sensing for global change research. *IEEE Trans. Geosci. Remote Sens.*, **36 (4)**, 1228–1249.

Kessler, E., 1969: *On the Distribution and Continuity of Water Substance in Atmospheric Circulations*, Vol. No. 32. Amer. Meteor. Soc., 84 pp. pp.

Kessler, E., 1995: On the continuity and distribution of water substance in atmospheric circulations. *Atmos. Res.*, 109–145.

Khairoutdinov, M. F. and Y. L. Kogan, 2000: A new cloud physics parameterization for large-eddy simulation models of marine stratocumulus. *Mon. Wea. Rev.*, **128**, 229–243.

Klein, S. A. and D. L. Hartmann, 1993: The seasonal cycle of low stratiform clouds. *J. Climate*, **6**, 1587–1606.

Kogan, Y. L., 2013: A cumulus cloud microphysics parameterization for cloud-resolving models. *J. Atmos. Sci.*, **70**, 1423–1436, doi:10.1175/JAS-D-12-0183.1.

Kogan, Y. L. and D. B. Mechem, 2014: A pdf-based microphysics parameterization for shallow cumulus clouds. *J. Atmos. Sci.*, **71**, 1070–1089, doi:10.1175/JAS-D-13-0193.1.

Krueger, S. K., G. T. McLean, and Q. Fu, 1995: Numerical simulations of the stratus-to-cumulus transition in the subtropical marine boundary layer. part i: Boundary-layer structure. *J. Atmos. Sci.*, 2839–2850.

Leach, M. J. and S. Raman, 1995: Role of radiative transfer in maintenance and destruction of stratocumulus clouds. *Atmos. Environ.*, **29 (16)**, 2009–2018.

Liu, Y. and P. H. Daum, 2004: Parameterization of the autoconversion process. part I: Analtical formulation of the kessler-type parameterizations. *J. Atmos. Sci.*, **61**, 2923–2940.

Liu, Y., P. H. Daum, and R. L. McGraw, 2005: Parameterization of the autoconversion process: Kessler-type, sundqvist-type, and unification. *Fifteenth ARM Science Team Meeting Proceedings*.

Manton, M. J. and W. R. Cotton, 1977: Parameterization of the atmospheric surface layer. *J. Atmos. Sci.*, **34**, 331–334.

McCaa, J. R. and C. S. Bretherton, 2004: A new parameterization for shallow cumulus convection and its application to marine subtropical cloud-topped boundary layers. part ii: Regional simulations of marine boundary layer clouds. *Mon. Wea. Rev.*, **132**, 883–896.

Mechem, D. B. and Y. L. Kogan, 2003: Simulatin the transition from drizzling marine stratocumulus to boundary layer cumulus with a mesoscale model. *Mon. Wea. Rev.*, **131**, 2342–2360.

Mechem, D. B. and Y. L. Kogan, 2008: A bulk parameterization of giant ccn. *J. Atmos. Sci.*, **65**, 2458–2466.

Mechem, D. B., P. C. Robinson, and Y. L. Kogan, 2006: Processing of cloud condensation nuclei by collision-coalescence in a mesoscale model. *J. Geophys. Res.*, **111**, D18 204, doi:10.1029/2006JD007183.

Mechoso, C. R., et al., 2014: Ocean-cloud-atmosphere-land interactions in the southeastern pacific: The vocals program. *Bull. Amer. Meteor. Soc.*, **95**, 357–375, doi:10.1175/BAMS-D-11-00246.1.

Medeiros, B., B. Stevens, I. M. Held, M. Zhao, D. L. Williamson, J. G. Olson, and C. S. Bretherton, 2008: Aquaplanets, climate sensitivity, and low clouds. *J. Climate*, **21**, 4974–4991.

Mellor, G. L. and T. Yamada, 1982: Development of a turbulence closure model for geophysical fluid problems. *Rev. Geophys.*, **20 (4)**, 851–875.

Morrison, H., J. A. Curry, and V. I. Khvorostyanov, 2005a: A new double-moment microphysics parameterization for application in cloud and climate models. part i: Description. *J. Atmos. Sci.*, **62**, 1665–1677.

Morrison, H., J. A. Curry, M. D. Shupe, and P. Zuidema, 2005b: A new double-moment microphysics parameterization for application in cloud and climate models. part ii: Single-column modeling of arctic clouds. *J. Atmos. Sci.*, **62**, 1678–1693.

Painemal, D. and P. Zuidema, 2011: Assessment of modis cloud effective radius and optical thickness retrievals over the southeast pacific with vocals-rex in situ measurements. *J. Geo. Res.*, **116**, doi:10.1029/2011JD016155.

Platnick, S., M. D. King, S. A. Ackerman, W. P. Menzel, B. A. Baum, J. C. Ridi, and R. A. Frey, 2003: The modis cloud products: Algorithms and examples from terra. *IEEE Transactions on geoscience and Remote Sensing*, **41**, 459–473.

Rahn, D. A. and R. Garreaud, 2010a: Marine boundary layer over the subtropical southeast pacific during vocals-rex - part 1: Mean structure and diurnal cycle. *Atmos. Chem. Phys.*, 4491–4506, doi:10.5194/acp-10-4491-2010.

Rahn, D. A. and R. Garreaud, 2010b: Marine boundary layer over the subtropical southeast pacific during vocals-rex - part 2: Synoptic variability. *Atmos. Chem. Phys.*, 4507–4519, doi:10.5194/acp-10-4507-2010.

Remer, L. A., et al., 2005: The modis aerosol algorithm, products, and validation. *J. Atmos. Sci.*, **62**, 947–973.

Rutledge, S. A. and P. V. Hobbs, 1983: The mesoscale and microscale structure and organization of clouds and precipitation in midlatitude cyclones. VIII: A model for the 'seeder-feeder' process in warm-frontal rainbands. *J. Atmos. Sci.*, **41**, 1185–1206.

Seifert, A. and K. D. Beheng, 2006: A two-moment cloud microphysics parameterization for mixed-phase clouds. part 2: Maritime vs. continental deep convective storms. *Meteor. Atmos. Phys.*, **92**, 67–82, doi:10.1007/s00703-005-0113-3.

Stevens, B., 2005: Atmospheric moist convection. *Annu. Rev. Earth Planent. Sci.*, **33**, 605–643, doi:10.1146/annurev.earth.33.092203.122658.

Stevens, B., W. R. Cotton, G. Feingold, and C.-H. Moeng, 1998: Large-eddy simulations of strongly precipitating, shallow, stratocumulus-topped boundary layers. *J. Atmos. Sci.*, **55**, 3616–3638.

Stocker, T. F., et al., 2014: Climage change 2013: The physical science basis. contribution of working group i to the fifth assessment report of the intergovernmental panel on climate change. Tech. rep., IPCC, 2013. doi:10.1017/CB09781107415324.

Toniazzo, T., S. J. Abel, R. Wood, C. R. Mechoso, G. Allen, and L. C. Shaffrey, 2011: Large-scale and synoptic meteorology in the south-east pacific during the observations campaign vocals-rex in austral spring 2008. *Atmos. Chem. Phys.*, **11**, 4977–5009, doi:10.5194/acp-11-4977-2011.

van Zanten, M. C., B. Stevens, G. Vali, and D. H. Lenschow, 2005: Observations of drizzle in nocturnal marine stratocumulus. *J. Atmos. Sci.*, **62**, 88–106.

Wang, S., L. W. O'Neil, Q. Jiang, S. P. de Szoeke, X. Hong, H. Jin, W. T. Thompson, and X. Zheng, 2011: A regional real-time forecast of marine boundary layers during vocals-rex. *Atmos. Chem. Phys.*, **11**, 421–437, doi:10.5194/acp-11-421-2011.

Wood, R., 2005: Drizzle in stratiform boundary layer clouds. Part II: Microphysical aspects. *J. Atmos. Sci*, **62**, 3034–3050.

Wood, R., 2006: Rate of loss of cloud droplets by coalescence in warm clouds. *J. Geophys. Res.*, **111**, D21 205, doi:10.1029/2006JD007553.

Wood, R., et al., 2011: The VAMOS Ocean–Cloud–Atmosphere–Land Study Regional Experiment (VOCALS–REx): Goals, platformas, and field operations. *Atmos. Chem. Phys.*, **11**, 627–654.

Wyant, M. C., et al., 2015: Global and regional modeling of clouds and aerosols in the marine boundary layer during vocals: the voca intercomparison. *Atmos. Chem. Phys.*, 153–172, doi:10.5194/acp-15-153-2015.

Zuidema, P., E. R. Westwater, C. Fairall, and D. Hazen, 2005: Ship-based liquid water path estimates in marine stratocumulus. *J. Geophys. Res.*, doi:10.1029/2005JD005833.